Mechanisms for Precipitation Enhancement in a North American Monsoon Upper-Tropospheric Trough

ANDREW NEWMAN* AND RICHARD H. JOHNSON

Department of Atmospheric Science, Colorado State University, Fort Collins, Colorado

(Manuscript received 18 August 2011, in final form 15 December 2011)

ABSTRACT

Tropical upper-tropospheric troughs (TUTTs), transient summertime disturbances over the Pacific and Atlantic Oceans, are also observed to frequently occur in the North American monsoon (NAM) region. However, unlike TUTTs over the Pacific and Atlantic, which feature a predominance of precipitation on the eastern flank of the disturbances, TUTTs in the NAM region have been shown to enhance precipitation on their western flank as they pass over the mountains of northern Mexico. To investigate this phenomenon, convection-permitting simulations are performed over the core NAM region for the 12–14 July 2004 TUTT event that occurred during the North American Monsoon Experiment (NAME). The effects of the TUTT are isolated using an approach that removes the vorticity anomaly associated with it. Six simulations, three with the TUTT and three without it, are then executed.

It is found that the mean of the TUTT simulations has increased surface–500-hPa and 700–400-hPa shear and that there is incrementally more convective available potential energy (CAPE) along the Sierra Madre Occidental (SMO). These differences lead to convective changes, with the TUTT simulations having more convection, larger maximum updraft velocities, and more precipitation in lower elevations. Overall, the TUTT simulation mean has about 15% more precipitation during the primary period of TUTT interaction with the northern SMO. There are also slight simulated microphysical differences that agree with nearby polarimetric radar observations. Finally, TUTT removal impacts the gulf surge event on 13 July via the convective modifications.

1. Introduction

Tropical upper-tropospheric troughs (TUTTs; Sadler 1967) are primarily mid- to upper-level circulation features observed over the Pacific and Atlantic Oceans. A positive vorticity maximum is typically found around 200 hPa with the corresponding circulation extending up to 100 hPa and down to near 700 hPa. A maximum negative temperature anomaly of a few kelvins is generally found around 300–400 hPa with a maximum warm anomaly around 125 hPa (Kelly and Mock 1982). The negative temperature anomaly can extend down to near 700 hPa (Kelly and Mock 1982; Whitfield and Lyons 1992). TUTT lows in the North American monsoon (NAM) region typically form from the North Atlantic TUTT, or thinning troughs associated with wave breaking over Texas or the western Gulf of Mexico on the downstream side of the upper-level monsoonal ridge (Thorncroft et al. 1993). They are then advected westward south of the monsoonal ridge, as depicted in Fig. 1 for the 12–14 July case observed during the North American Monsoon Experiment (NAME). TUTT lows in the NAM region are very similar in vertical structure to those found in other areas of the tropics (Finch and Johnson 2010).

However, unlike TUTT lows elsewhere, which have precipitation primarily on the eastern side of the circulation center (Sadler 1967; Kelly and Mock 1982), TUTT lows in the NAM region have been shown to have enhanced precipitation/convection on the western flank (Douglas and Englehart 2007; Bieda et al. 2009; Finch and Johnson 2010). Douglas and Englehart (2007) developed a climatology of transient upper-level circulations in the NAM and documented the precipitation around TUTT lows. They found that rainfall is maximized to the

* Current affiliation: National Center for Atmospheric Research,[+] Boulder, Colorado.

[+] The National Center for Atmospheric Research is sponsored by the National Science Foundation.

Corresponding author address: Andrew Newman, NCAR-RAL, Boulder, CO 80307.
E-mail: anewman@ucar.edu

DOI: 10.1175/JAS-D-11-0223.1

© 2012 American Meteorological Society

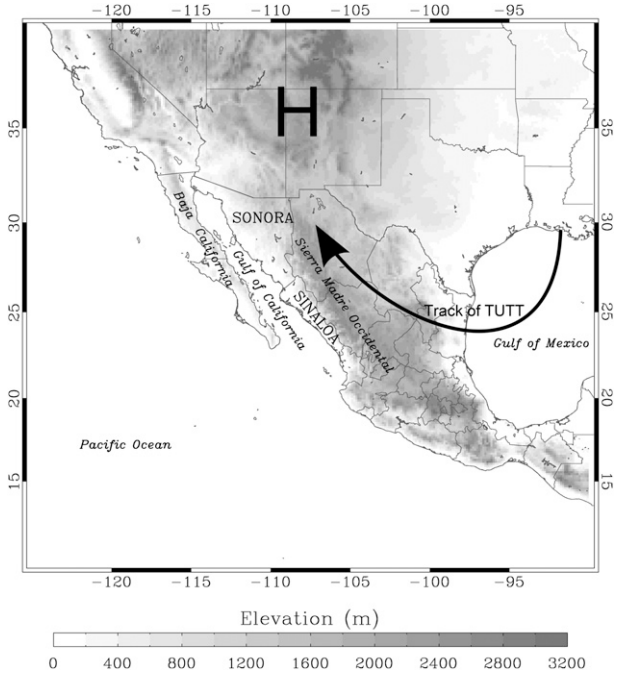

FIG. 1. Overview of North American monsoon region for the 12–14 Jul 2004 TUTT case. Geographic and political boundaries are noted on the map. Arrow indicates path of the 200-hPa TUTT center and H the general center of the 200-hPa monsoon ridge.

west of the low center, but they did not give an explanation for the observed precipitation pattern. Bieda et al. (2009) also documented statistically significant increases in lightning frequency and precipitation associated with TUTT low passages over many areas in the northern core NAM region.

Pytlak et al. (2005) developed a conceptual model of TUTT lows in the NAM region and proposed that upper-level diffluence in the front-right quadrant (west of the low center) leads to an increase in convection in that region. However, is that diffluence actually tied to divergence and rising motion? Finch and Johnson (2010) examined a TUTT low during NAME and concluded that convection over the Sierra Madre Occidental (SMO; Fig. 1) seems to be modulated by the TUTT low through changes in the midlevel shear. The 700–400-hPa shear magnitude increases and the shear vector changes direction such that it is more perpendicular to the SMO. This situation creates an environment where convection can organize, grow upscale, and propagate off the SMO more readily than on days without a TUTT low present to the east of the SMO. Finch and Johnson (2010) largely refute the hypothesis of Pytlak et al. (2005), but their study examines thermodynamic data from NAME with limited spatial and temporal resolution. Changes in the storm environment and/or organization may also lead to microphysical changes that may influence lightning and precipitation, features that have heretofore received little study.

To better understand the mechanisms by which TUTT lows in the NAM region enhance convection on their western flank, six regional simulations with explicit convection are performed for a TUTT low[1] case during NAME. Three simulations include the TUTT low, while the other three have the low largely removed from the initial conditions. The procedure involves the use of a vorticity anomaly removal algorithm, which removes specified vorticity centers in model initial condition. Comparisons of momentum, thermodynamic, and other fields between the simulations provide an opportunity to investigate the specific impacts of the TUTT low on wind shear, stability, and microphysical parameters that lead to enhanced precipitation. The impacts of these convective differences on the evolution of a corresponding Gulf of California moisture surge event (Hales 1972; Brenner 1974) are also discussed.

2. Simulation methodology

The Advanced Research Weather Research and Forecasting (ARW-WRF) atmospheric model version 3.3.1 (Bruyere et al. 2010) is used employing one high-resolution domain of 2000×2320 km^2 dimension (Fig. 2), a horizontal grid spacing of 4 km (501×581 points), and 55 vertical levels between the surface and 100 hPa. The vertical grid is stretched such that it has seven levels in the lowest 1 km to a constant height change Δz of approximately 340 m in the upper troposphere. In all simulations the Rapid Radiative Transfer Model longwave, Dudhia shortwave, Noah land surface model, and Quasi-Normal Scale Elimination (QNSE) surface and boundary layer schemes are used. Three microphysics schemes covering a range of heritages and complexities are used: the Thompson hybrid single-moment scheme (Thompson et al. 2008), which was initially based on Reisner et al. (1998); the WRF Single-Moment 6-Class Scheme (WSM6), which is a Lin-type scheme (Lin et al. 1983; Hong and Lim 2006); and the Morrison double-moment scheme (Morrison et al. 2005, 2009). Multiple simulations are done in an effort to address the various convective evolution solutions seen using different

[1] Sadler's (1967) definition of a TUTT low strictly regarded upper-tropospheric troughs that originated from certain favored locations (e.g., the Caribbean upper-tropospheric trough region). While the TUTT low in this case did not originate in one such area, it is referenced as a TUTT low because it is an upper-tropospheric trough in the same vein as Sadler's TUTT lows except for its initiation location.

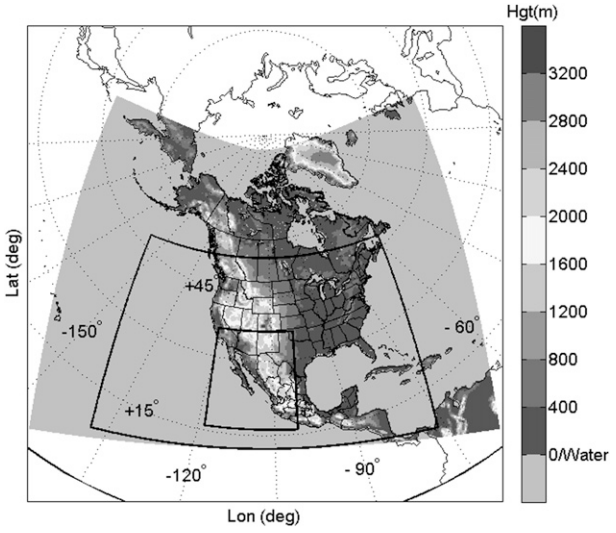

FIG. 2. The NARR domain (shaded region) along with the 20-km (outer thick line) and 4-km (inner thick line) domains.

microphysics parameterizations and give some robustness to the results. Three simulations for each initial condition option (TUTT and No_TUTT) do not represent a sufficient sample size to produce ensemble statistics, but they do lend support to the subsequent results because the different realizations have the same signals in them. For all figures, the mean of the three simulations for each initial option is presented unless otherwise noted.

The North American Regional Reanalysis (NARR) is used for all initial and boundary conditions. The NARR is produced 8 times daily (3-h intervals) with 29 vertical levels from 1000 to 100 hPa at 32-km horizontal resolution (Mesinger et al. 2006). All simulations are initialized at 0600 UTC 12 July and integrated until 0000 UTC 14 July. Analysis begins at 1600 UTC 12 July, giving 10 h of spinup time for WRF to generate the appropriate higher-resolution circulation and precipitation features. This was done in an effort to focus analysis on one diurnal cycle having a strong TUTT low influence: 12–13 July. To remove the TUTT low (TUTT for brevity) from the NARR data, a 20-km horizontal grid space domain covering a large subset (7400×4900 km^2) of the NARR was created (Fig. 2). The WRF Preprocessing System (WPS) is used to create 3-h analyses on the 20-km domain grid and the domain was selected such that the TUTT circulation resided entirely inside the domain at the initial time. A modified version of the tropical cyclone (TC) bogus scheme is then used to remove the vorticity, height, and temperature anomalies associated with the TUTT. The TC bogus scheme removes a vorticity center in WPS data files that are then used to create new initial and boundary conditions.

The standard bogussing scheme begins by searching for the vortex center in the 1000-hPa analysis data as defined by the maximum in relative vorticity within a 400-km radius of a point specified by the user (Fredrick et al. 2009, www.mmm.ucar.edu/wrf/users/workshops/WS2009/abstracts/P1-05.pdf). For this simulation the actual vortex center was specified because the relative vorticity of a TUTT is much more diffuse than a TC and the search algorithm may struggle finding the correct center of the TUTT. The vortex center was determined through examination of the NARR relative vorticity and wind fields. The scheme then removes the vortex from each level, starting at the surface to the model top. In this case, TUTTs are upper-level features so the removal scheme was modified to only remove relative vorticity above 600 hPa, as this TUTT was relatively weak below this level (Finch and Johnson 2010). This step also avoids the complication of terrain (SMO) below approximately 750 hPa. The standard bogus scheme removes all relative vorticity and divergence within a 300-km radius from the vortex center, but for this application the radius is increased to 650 km because of the larger scale of the TUTT. The relative vorticity, divergence, height, and temperature perturbations are removed using relationships between streamfunction and vorticity, velocity potential and divergence, geostrophic vorticity and geopotential height, and the hydrostatic approximation, respectively.[2]

Once the vortex is removed from all the NARR fields on the 20-km domain for all times included in the simulations, initial and boundary conditions are created for the 4-km domain (Fig. 2) and then the six simulations are performed. Comparisons will then be made examining the impact of TUTT removal on the simulated convective and surge evolution. Various difference fields are used to highlight the important features influencing any evolution differences between the two runs. All the difference fields are taken as the difference between the mean of the TUTT and No_TUTT simulations unless otherwise noted. Figure 3 shows 250-hPa wind for the runs with the TUTT included (TUTT) and the simulations with the TUTT removed (No_TUTT) at 1600 UTC 12 July. It can be seen that the TUTT removal algorithm successfully removed the TUTT. Most importantly the 4-km simulations are able to successfully bring the TUTT circulation into the domain and sustain the distinct differences resulting from the TUTT removal.

[2] The TC bogus scheme removes the rotational and divergent wind because it is designed for tropical cyclones. In our case the divergent wind is still removed, but the effects are expected to be small because the TUTT is a larger scale, nearly balanced feature.

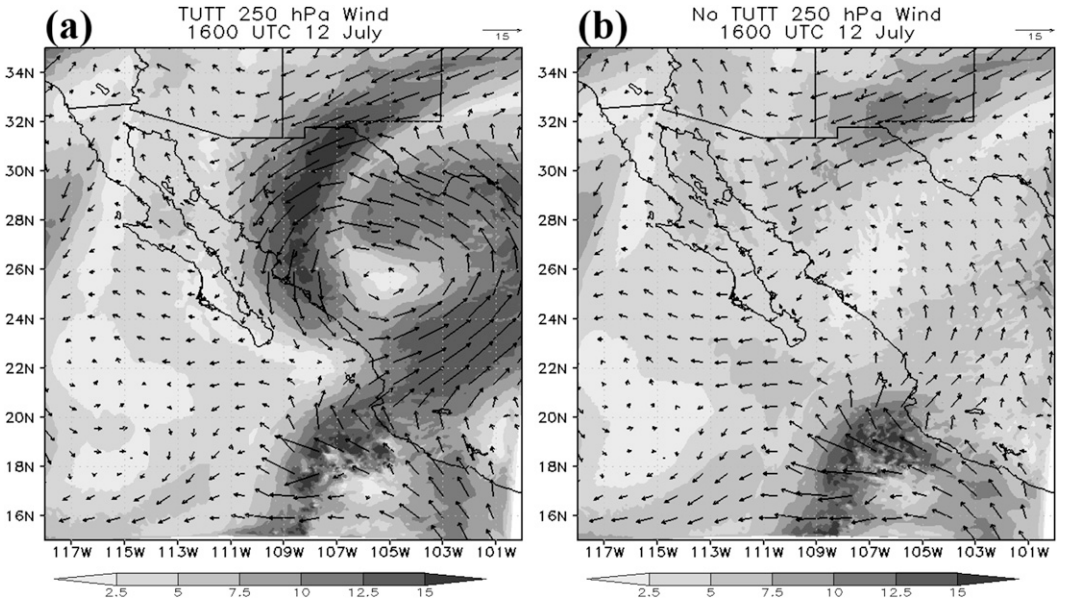

FIG. 3. 250-hPa wind (m s^{-1}) magnitude and vectors at 1600 UTC 12 Jul for the (a) TUTT and (b) No_TUTT simulations.

3. Meteorological overview

The TUTT simulated in this work originated from a thinning shortwave trough that had crested the axis of the subtropical monsoon high located over New Mexico and Colorado around 0000 UTC 9 July 2004 (Finch and Johnson 2010). By 1200 UTC 9 July the TUTT has a closed height contour at 200 hPa and a complete cyclonic circulation around the low center (Fig. 4a). Over the next 24 h the TUTT deepens and intensifies while moving south-southeast to near 23°N, 97°W at 1200 UTC 10 July (Fig. 4b). The TUTT then begins to move west-northwest while maintaining a similar intensity at 200 hPa through about 1200 UTC 12 July (Figs. 4c,d). Between 1200 UTC 12 July and 0600 UTC 13 July the TUTT weakens while moving nearly due north to near 29°N, 104°W at 0600 UTC 13 July. The TUTT dissipates shortly after 0600 UTC 13 July (Finch and Johnson 2010). The simulation reproduces the location of the TUTT well on 12–13 July (cf. Figs. 3a and 4d).

The track of this particular TUTT is such that the western semicircle of the TUTT interacts and enhances convection over the SMO over several days as shown in Finch and Johnson (2010). Figure 5 shows the *Geostationary Operational Environmental Satellite-10* (*GOES-10*) enhanced IR images from around 0400 UTC 10–13 July. Finch and Johnson (2010) show that the TUTT does not begin to influence the mid- and upper-level winds along the SMO until 11 July with the most significant changes noted on 12 and 13 July. Convection can be seen to be enhanced via a greater area of cloud tops colder than −40°C on 11–13 July (Figs. 5b–d) as compared to 10 July (Fig. 5a) and more notably as compared to days prior to 10 July (not shown). The most extensive convection is seen on 12 and 13 July along the central and northern SMO, north of about 24°N (Figs. 5c,d), corresponding to the regions of strongest midlevel shear (Finch and Johnson 2010).

Finally the diurnal cycle of convection is represented in a reasonable manner in the simulations. Figure 6 displays the areal coverage of precipitation in the NAME radar network region (Lang et al. 2007) for the observations and the TUTT and No_TUTT simulations using the Thompson microphysics scheme. The diurnal cycle of convection is captured in the simulation reasonably well; however, the simulations have their peak activity about 3 h early, which agrees with previous simulations in the NAM region (Li et al. 2008). The Morrison and WSM6 scheme simulations have very similar diurnal cycles. All simulations have reasonable placement of convection along the SMO determined through comparisons of simulated cloud-top and radar reflectivity images to those observed (not shown).

4. Convection enhancement mechanisms

a. Divergence mechanism

Prior studies of TUTT locations outside the core NAM region found enhanced rising motion and precipitation generally on the eastern side of the circulation (Erickson 1971; Kelly and Mock 1982; Whitfield and

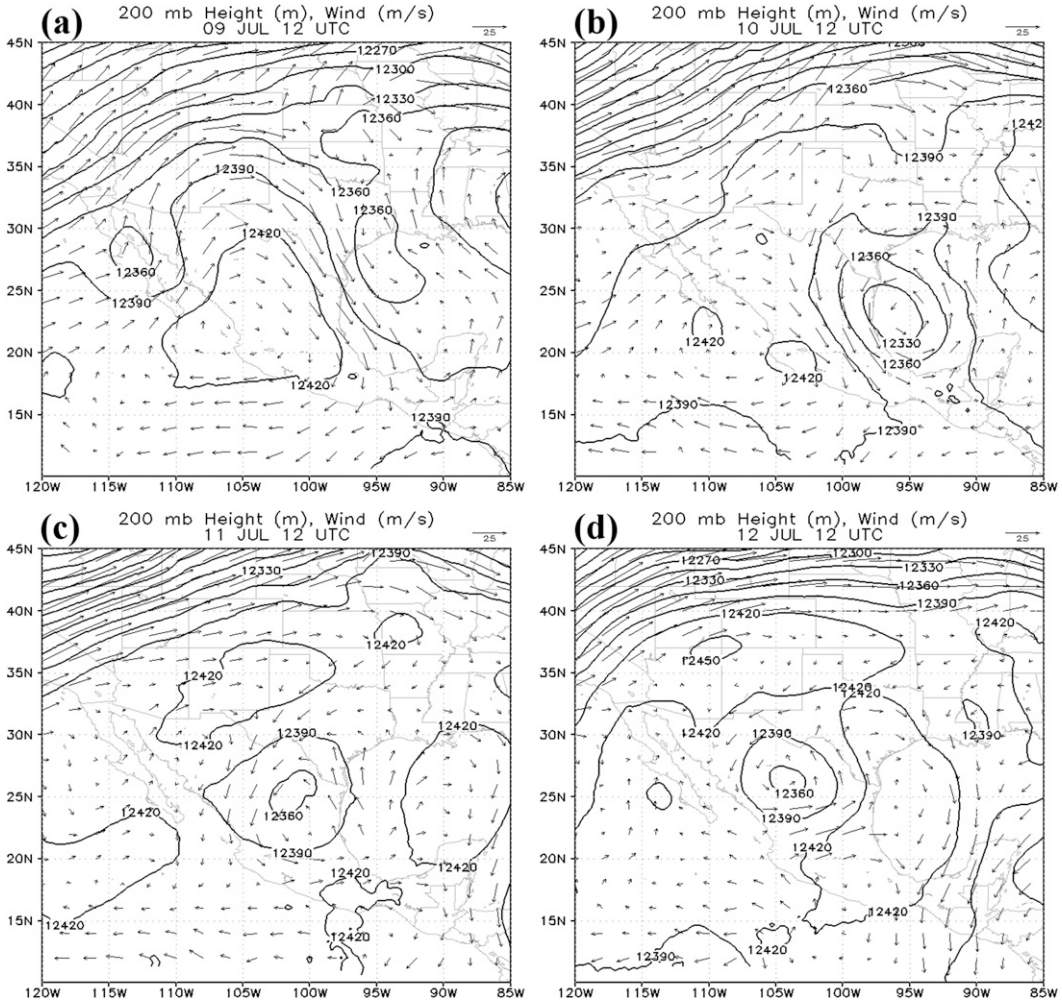

FIG. 4. Observed 200-hPa height (contours; m) and wind vectors (arrows; m s^{-1}) from 1200 UTC 9 Jul to 1200 UTC 12 Jul.

Lyons 1992; Chen and Chou 1994). Pytlak et al. (2005) suggested that TUTTs in the NAM region have enhanced upper-level diffluence, divergence, and rising motion in the northwest quadrant of the TUTT. Finch and Johnson (2010) examined the TUTT modeled herein using the quasigeostrophic (QG) omega equation and found QG-forced sinking motion in the 700–300-hPa layer to the west of the TUTT center when using the TUTT composite fields, which agrees with the TUTT studies outside the NAM region. The TUTT simulations do enhance diffluence[3] in the northwest quadrant of the TUTT, which supports the first assertion in Pytlak et al. (2005) (Figs. 7a,b). However, the divergence pattern is disorganized in the northwest quadrant of the TUTT with no clear association of divergence or rising motion with the diffluent area (not shown). Also, slightly enhanced midlevel sinking motion to the northwest of the TUTT (Figs. 7c,d; over the northern SMO, near 28–30°N, 110°W) before convective initiation is present in the TUTT simulations along the SMO. Therefore, another mechanism must be responsible for the enhanced precipitation and convection over the SMO when a TUTT is present to the east of the SMO axis, in agreement with Finch and Johnson (2010).

b. *Shear mechanism*

Finch and Johnson (2010) found that there is a correlation between enhanced convection along the SMO and the 700–400-hPa mean flow and bulk shear. They show that areas with enhanced 700–400-hPa mean flow and bulk shear have colder cloud tops and enlarged canopy

[3] Diffluence is calculated by finding the two components of divergence in natural coordinates with the second component being diffluence. See Eq. (3.1.35) of Bluestein (1992).

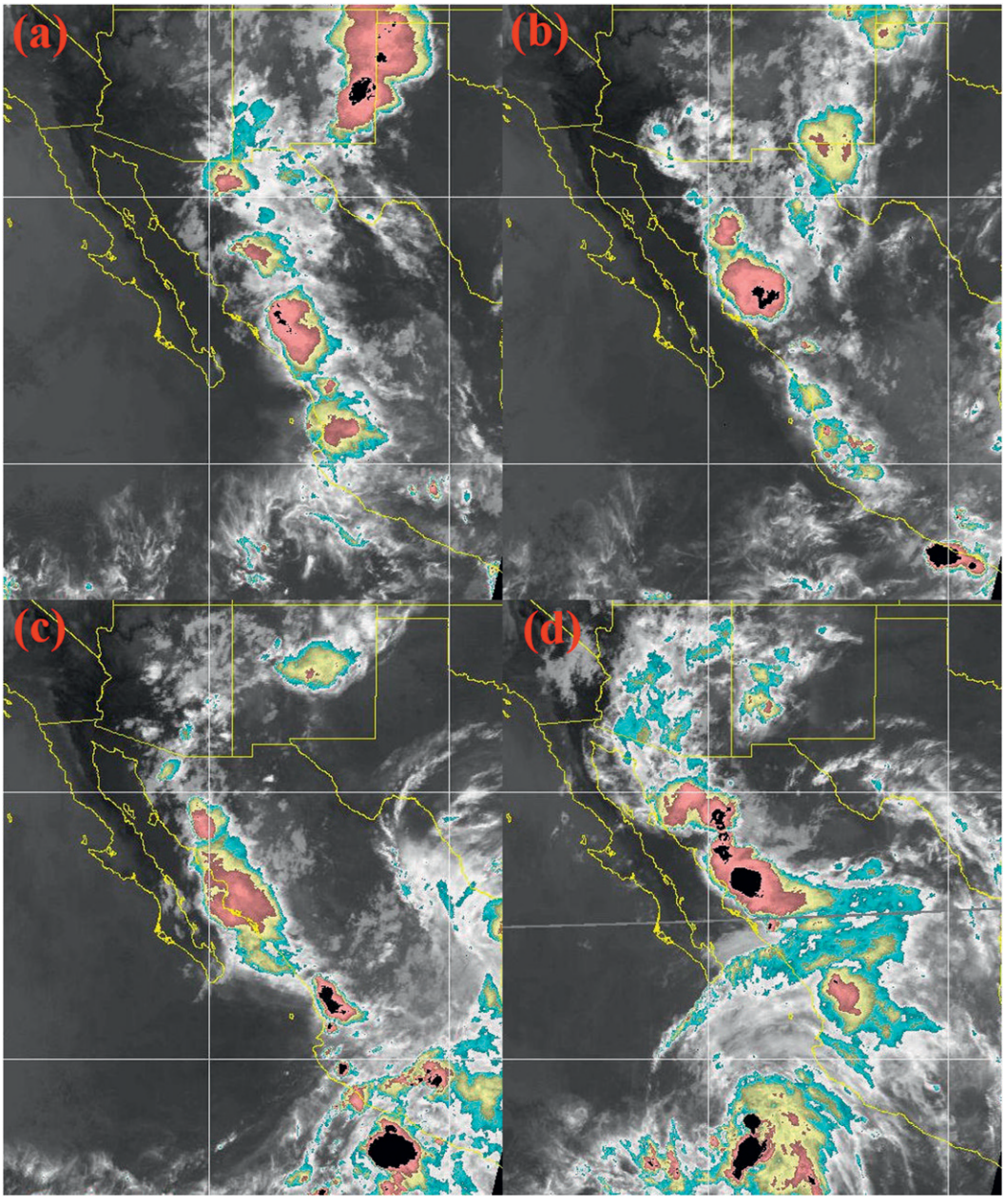

FIG. 5. GOES infrared color enhanced brightness temperatures (K) over the core NAM region at (a) 0400 UTC 10 Jul, (b) 0400 UTC 11 Jul, (c) 0400 UTC 12 Jul, and (d) 0400 UTC 13 Jul.

areas (their Figs. 11 and 12). They propose the changes in the midlevel flow create a more favorable environment for convection to organize, move off the SMO, and persist longer than on non-TUTT days. Lang et al. (2007) suggest days with increased shear in the NAM have increased convective organization through cold pool–shear interaction described by Rotunno et al. (1988). This interaction considers horizontal vorticity interactions between the updraft, cold pool, and environment. As the vorticity contributions from the updraft and environment become more balanced with the cold pool vorticity, the updraft becomes more upright and stronger (Weisman and Rotunno 2004). Weisman and Rotunno (2004) show that for a given shear depth, increasing the surface-based or elevated shear results in squall systems that have larger maximum vertical velocities and produce more rainfall. The most drastic increases in precipitation generally occur when small shear magnitudes are increased, rather than cases having large shear magnitudes increasing further (Weisman and Rotunno 2004).

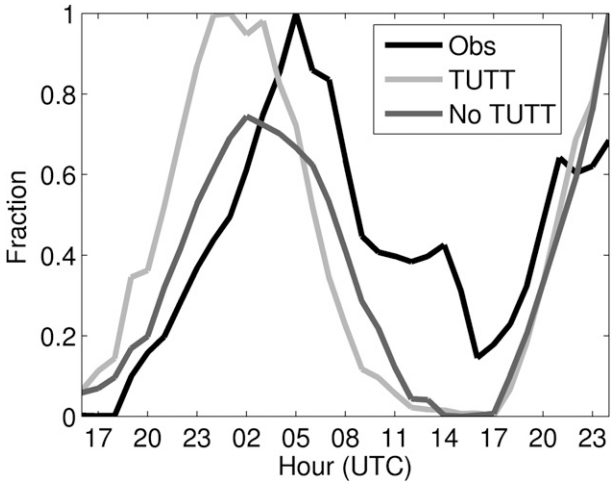

FIG. 6. Fractional coverage area normalized by the maximum coverage area in the NAME radar network domain (Lang et al. 2007) for the observations and TUTT, and No_TUTT simulations using the Thompson microphysics scheme from 1600 UTC 12 Jul to 0000 UTC 14 Jul.

Figure 8 shows the 700–400-hPa (Fig. 8a) and the surface–500-hPa (Fig. 8b) difference fields for bulk shear at 1600 UTC 12 July. The TUTT mean has a large area of increased 700–400-hPa bulk shear (red shading), generally 1–5 m s^{-1} more 700–400-hPa bulk shear with areas near 28°N, 108°W being up to 9 m s^{-1} greater. These values are very similar to those of Finch and Johnson (2010) at 0000 UTC 13 July when comparing to the mean NAME flow. The 700–400-hPa shear vectors in the TUTT simulations are also more perpendicular to the SMO in the same region (Fig. 8a). Also, the TUTT simulations have surface–500-hPa shear increases of 1–5 m s^{-1} (red shading, Fig. 8b) over the northern SMO during convective initiation and propagation on 12–13 July and the shear vector is again generally more perpendicular to the SMO in the TUTT simulations. This suggests the environment is more favorable for convective organization and propagation, from a shear standpoint, in the northern SMO in the TUTT simulations (Smith and Gall 1989; Farfán and Zehnder 1994; Weisman and Rotunno 2004; Lang et al. 2007). Over the northern SMO between 28° and 32°N, the TUTT runs have also increased the 700–400-hPa mean flow of up to 2 m s^{-1}, which would, in most cases, also increase storm motion and propagation off the SMO (Byers and Braham 1948; Chappell 1986; Corfidi 2003).

THERMODYNAMIC CONSIDERATIONS

To rule out thermodynamic changes as the convective enhancement mechanism, sounding analysis at two coastal sites (Los Mochis and Bahia Kino) was performed by Finch and Johnson (2010). They argue that there are insignificant changes in CAPE related to upper-level cooling from the TUTT and show that nearly all CAPE changes over the life of the TUTT at these two sites are related to near surface moisture changes associated with a 13–14 July Gulf of California (GoC) surge event. However, they do note that slight midlevel cooling took place between 12–13 July at the two sites, which produced minor changes in CAPE they associated with the TUTT. Figure 9 displays mass-weighted difference fields for potential temperature (Fig. 9a), specific humidity (Fig. 9b), wind (Fig. 9c), and the difference in 90-hPa mixed layer CAPE (Fig. 9d) at 1600 UTC 12 July between the surface and 850 hPa. The largest magnitude differences for all fields are found over the GoC and Baja Peninsula and are due to slight differences in convective evolution early in the simulations. The convective influences on the difference fields appear to be minimal along the SMO from examination of the time evolution of the difference fields near the SMO (not shown). By 1600 UTC 12 July the simulations have minimal potential temperature differences with the TUTT mean being around 0.5 K cooler in the lowest 150 hPa along the northern SMO (Fig. 9a; 28°–31°N, 108°–111°W). The TUTT simulations have slightly less moisture along the coastal plain but more moisture above 500 m along the SMO, especially in the northern SMO (29°–31°N, 108°–111°W). The latter is due to the TUTT simulations having slightly stronger low-level flow directed into the SMO before 1600 UTC. The TUTT mean has slightly weaker low-level flow south of 30°N, but the TUTT mean wind vectors are slightly more perpendicular to the SMO at 1600 UTC (Fig. 9c).

The most interesting of the fields in Fig. 9 is the lowest 90-hPa mixed layer CAPE difference field. At 1600 UTC the TUTT simulations have consistently higher CAPE (up to several hundred J kg^{-1}) over most of the higher elevations along the SMO. The CAPE differences are primarily due to increased low-level moisture in the northern SMO (28°–31°N, 108°–111°W; Fig. 9b) and mid- to upper-level cooling along the central and southern SMO (22°–27°N, 105°–109°W; not shown). The central and southern SMO are much closer to the TUTT center at this time where the largest differences in mid- and upper-level temperatures reside. Figure 10 gives an example sounding from the northern SMO (30°N, 110°W) to highlight the slight differences in the temperature and moisture between the TUTT and No_TUTT simulations. The TUTT sounding has about 100 J kg^{-1} more CAPE. Surface-based thermodynamic diagram parcel paths are nearly the same but not identical (not shown) with the TUTT parcel having a slightly lower lifted condensation level (LCL) and a warmer cloud base. This

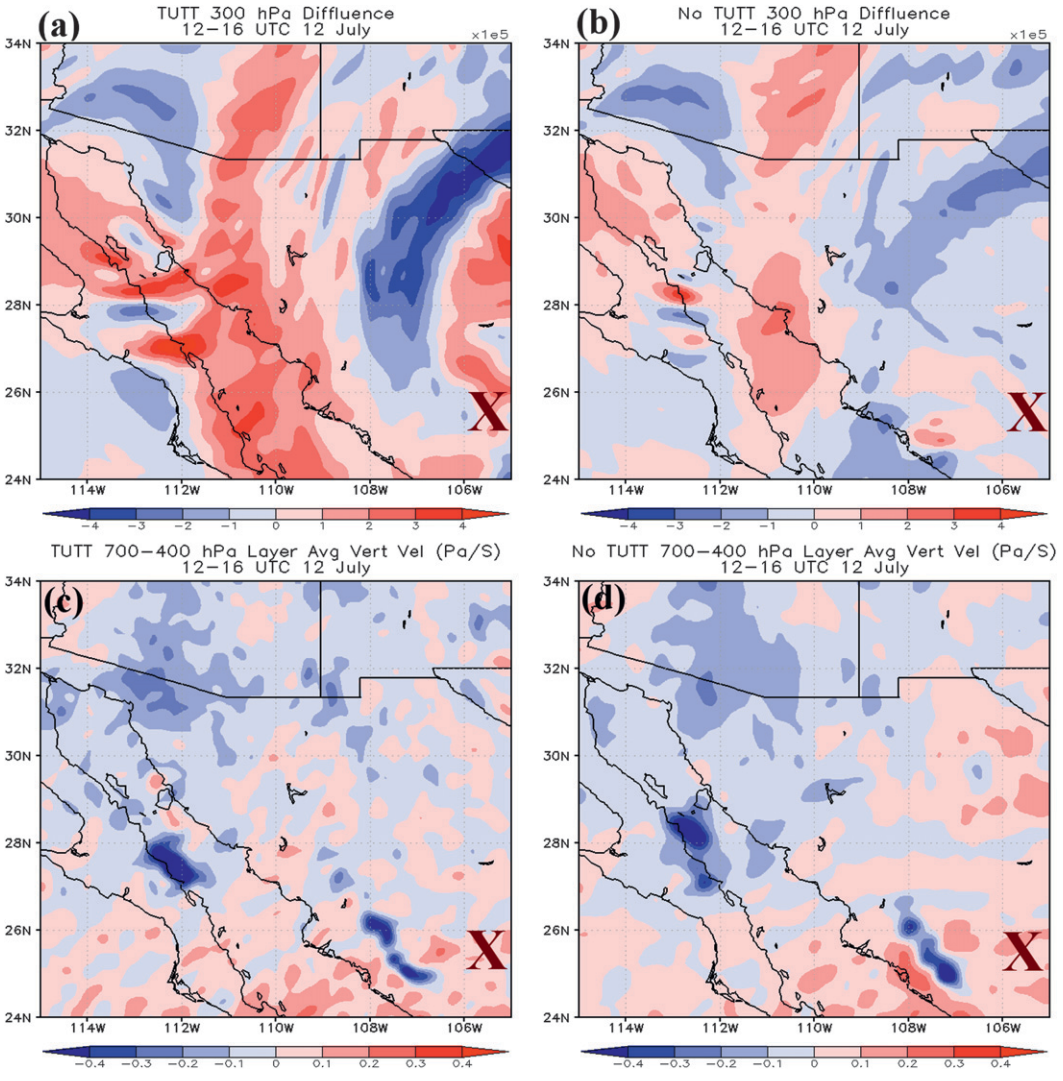

FIG. 7. (a),(b) 300-hPa diffluence ($\times 10^{-5}$ s^{-1}) and (c),(d) 700–400-hPa mass- and time-weighted vertical velocity (Pa s^{-1}) for the (a),(c) TUTT and (b),(d) No_TUTT simulations from 1200 to 1600 UTC 12 Jul. The boldface red X denotes the approximate TUTT center.

combined with the small temperature differences results in the CAPE difference.

While Finch and Johnson (2010) indicate that there are no significant differences in surface-based CAPE related to the TUTT at the two coastal sites (they find temporal changes in CAPE, but relate them to the GoC surge), they do find slight mid- and upper-level cooling. This cooling would be expected to be greater along the SMO, closer to the TUTT center. There may also be unobserved moisture differences (NAME soundings were along the coast and east of the SMO crest) attributable to the TUTT along the complex terrain of the SMO foothills as well. Only slight differences in the lowest 150-hPa mean flow in these simulations results in moisture differences of up to 2 g kg^{-1} in certain valleys (Fig. 9b). These differences in temperature, moisture, and the resultant CAPE are more significant in areas of smaller CAPE, like the SMO foothills, and could impact convective intensity and microphysical characteristics.

c. *Combined mechanism*

The subtle changes in CAPE during convective initiation result in larger maximum vertical velocities in the convective elements for the TUTT simulations. Figure 11 shows a time series of maximum vertical velocity for all grid points between 28° and 33°N and 113° and 107°W for the mean of the TUTT and No_TUTT simulations. The southern boundary at 28°N corresponds with the southern boundary of the analysis performed in Bieda et al. (2009). It is evident that in the TUTT simulations,

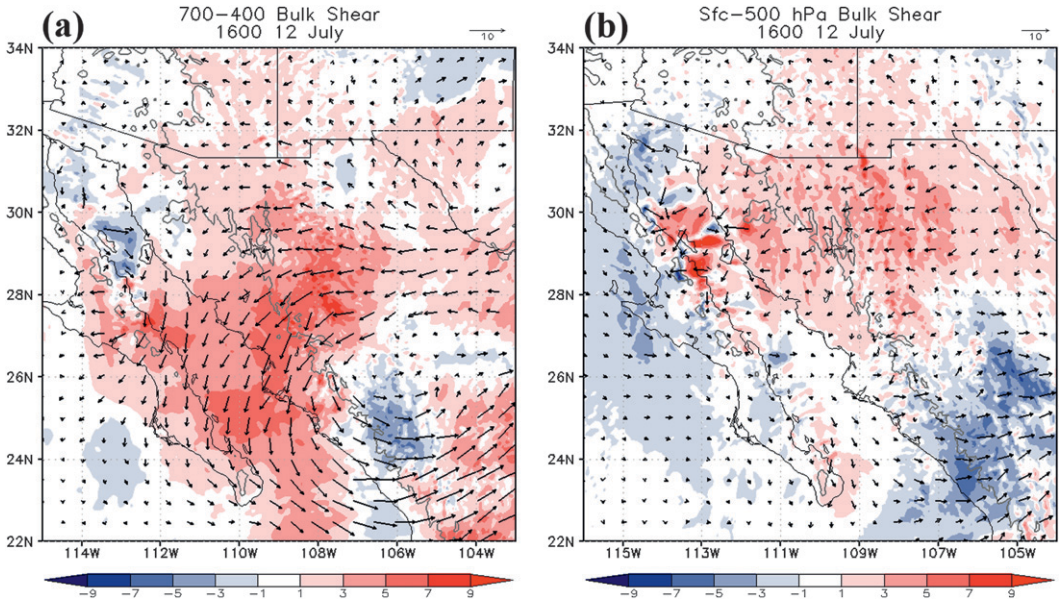

FIG. 8. TUTT − No_TUTT (a) 700–400-hPa and (b) surface–500-hPa bulk shear (m s^{-1}). The arrows display the shear difference vector and the light gray contour is the 750-m terrain elevation.

deep convection begins in earnest by 1700 UTC with a rapid increase in maximum vertical velocities, while the No_TUTT cases are delayed by about 1 h (Figs. 6 and 11). CAPE can be used as an upper bound for vertical velocity from parcel theory (Crook 1996). This assumption neglects many processes such as precipitation loading, entrainment of drier air, etc., but there is a strong correlation between CAPE and simulated maximum vertical velocity (Crook 1996). In the initial stages of convection, shear imposes a mean inhibition to the growth of convective elements due to the increased entrainment of drier, less energetic air into the updraft (Cotton et al. 2010). Weisman and Rotunno (2004) also indicate that maximum vertical velocities are less in more strongly sheared environments for the first 1–2 h. This reasoning implies the TUTT simulations should have weaker initial updrafts as compared to the No_TUTT simulations given equal CAPE. Accounting for the delayed convective onset in the No_TUTT simulations (~1 h later), the TUTT simulations do have weaker maximum vertical velocities for the first several hours of convection (1600–1900 UTC; cf. 1900 UTC No_TUTT and 1800 UTC TUTT in Fig. 11) in an environment with slightly stronger shear and larger CAPE and at a time when precipitation loading should be less drastic in both simulations. This suggests that the increased shear is overwhelming the increased CAPE in the TUTT simulations for the first couple hours of convective development. At the peak intensity, the TUTT simulations have maximum vertical velocities several meters per second greater than that of the No_TUTT simulations, in agreement with the results of Weisman and Rotunno (2004) and Crook (1996).

After the initial convective development, shear is also important in organizing, maintaining, and increasing precipitation in convection (Rotunno et al. 1988; Weisman and Rotunno 2004; Coniglio et al. 2006). The northern SMO has enhanced shear along the northern SMO (Fig. 8) and stronger 700–400-hPa mean flow perpendicular to the SMO in the TUTT simulations. If shear is helping to sustain and organize convection, that region should experience more total rainfall than the No_TUTT simulations (Weisman and Rotunno 2004; Bryan et al. 2006; Coniglio et al. 2006) and have more precipitation farther from the SMO due to the enhanced mean flow "steering" convection farther west (Chappell 1986; Corfidi 2003). Figure 12 displays the accumulated precipitation difference field for the time period 1800 UTC 12 July–1200 UTC 13 July. This period extends from just after convective initiation through complete dissipation over the northern SMO. The TUTT simulations appear to produce more precipitation in this region, especially in the lower terrain.

Table 1 gives the total precipitation for the region for the mean of the TUTT and No_TUTT simulations, and the total precipitation broken down into three categories distinguished by terrain height: low, middle, and high. The high terrain is defined by areas greater than 1000 m, the middle terrain is bracketed between 500 and 1000 m, and the low terrain is below 500 m. This breakdown gives a more quantitative view of the ability of convection to propagate off the high peaks. Overall, the

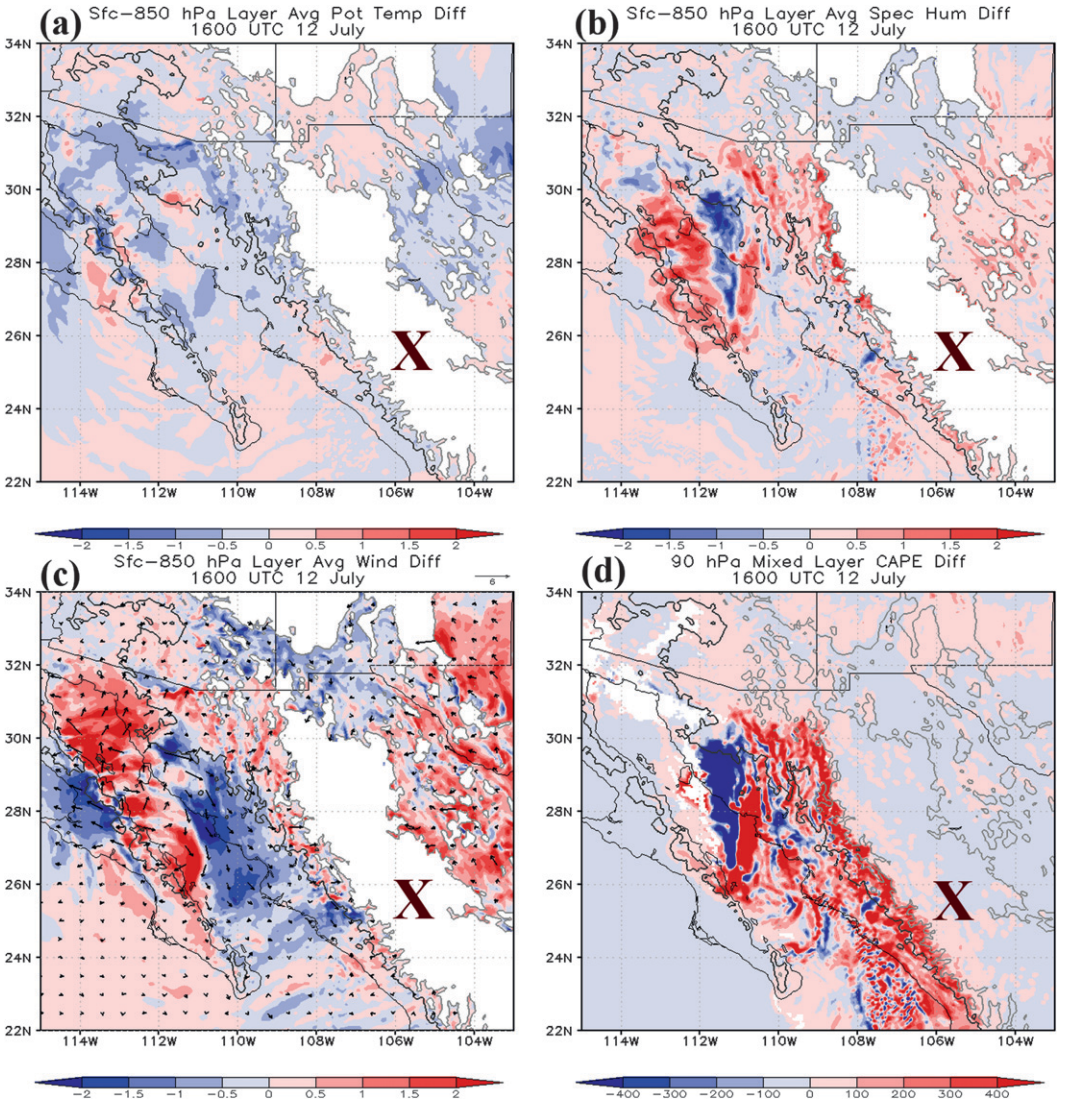

FIG. 9. TUTT − No_TUTT (a) surface–850-hPa mass-weighted potential temperature (K), (b) surface–850-hPa specific humidity (g kg^{-1}), (c) surface–850-hPa wind (m s^{-1}), and (d) the lowest 90-hPa mixed layer CAPE (J kg^{-1}). The three black/gray contours denote the 0-, 500-, and 1500-m terrain contours (lighter is higher). The white areas in (a)–(c) denote areas above 850 hPa, while in (d) they denote areas with mixed layer convective inhibition greater than 200 J kg^{-1}. The boldface red X denotes the approximate TUTT center.

average accumulated precipitation of the TUTT simulations is 16% larger than the No_TUTT mean. For the three (low to high) terrain ranges, the TUTT simulations produce 125% more, 23% less, and 16% more precipitation, respectively. The changes in the percentage differences strongly suggest the TUTT-simulated convection propagates more readily off the SMO. The TUTT simulations generate more precipitation at higher elevations, but less at middle elevations. Also, the TUTT runs precipitate over a larger area than the No_TUTT simulations and have a higher mean precipitation accumulation of 4.4 versus 4.17 mm for all areas with precipitation in Fig. 12.

The conclusion drawn from these simulations is that the No_TUTT simulations produce slightly less initial convection, that convection does not propagate as fast toward the lower terrain, and that it precipitates heaviest over the slopes of the SMO. When reaching the low terrain, the No_TUTT simulated convection decays away while the TUTT convection continues westward. Examination of simulated reflectivity finds that the TUTT simulations have more short line segments versus individual convective elements and that they propagate farther west. To illustrate this, Fig. 13 displays simulated radar reflectivity from the Morrison scheme TUTT and No_TUTT simulations at 2100 UTC 12 July and 0000

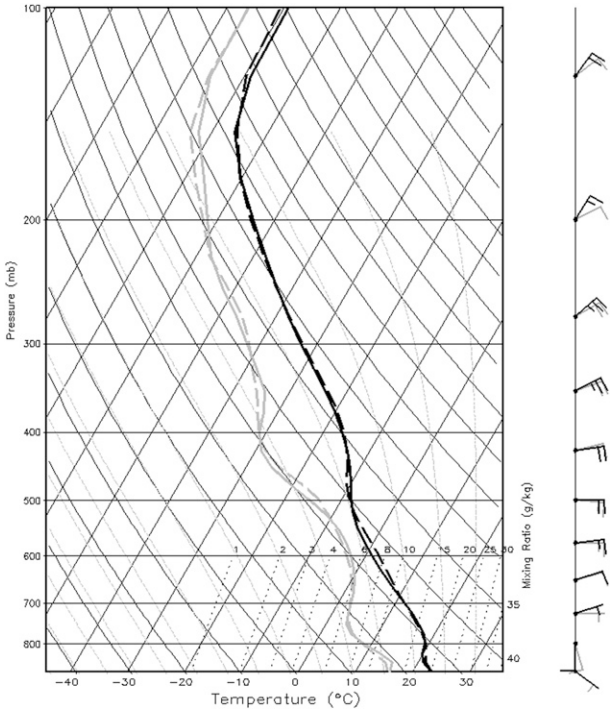

FIG. 10. TUTT (solid) and No_TUTT (dashed) temperature (black; °C) and dewpoint (gray; °C) sounding for 30°N, 110°W at 1600 UTC 12 Jul. Wind barbs follow standard convention [knots (kt); 1 kt = 0.51 m s^{-1}] with black barbs and gray barbs for the TUTT and No_TUTT simulations, respectively.

and 0300 UTC 13 July. The TUTT-simulated convection has a more linear appearance at 2100 and 0000 UTC along with more areal coverage. At 0300 UTC the most intense remnant convection is located farther west than the No_TUTT simulation.

d. Microphysical aspects

With differing initial CAPE and shear profiles, it is likely that the microphysics of convection in the two simulations differ, and in potentially significant ways. Figure 11 shows that convection in the TUTT simulation is more vigorous than the No_TUTT run for the few hours near peak convective intensity. Besides enhancing precipitation, the analysis of Bieda et al. (2009) shows that TUTTs modify the National Lightning Detection Network (NLDN; Cummins et al. 1998) cloud-to-ground (CG) lightning climatology in the northern SMO, north of 28°N. When a TUTT passage occurs, there are more CG strikes along the northern SMO than on non-TUTT days (Bieda et al. 2009). One conclusion would be that since there is more organized convection and more precipitation over a larger area there would naturally be more CG lightning. It is also possible that microphysical differences between the storms influenced by a TUTT further enhance CG lightning strikes.

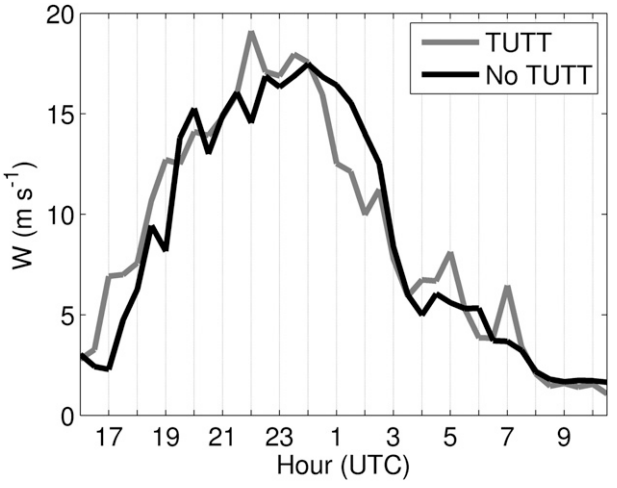

FIG. 11. Maximum vertical velocity (m s^{-1}) for the (a) TUTT and (b) No_TUTT simulations between 28° and 33°N and 113° and 107°W for 1600 UTC 12 Jul–1000 UTC 13 Jul.

It is generally agreed that ice processes are critical to the electrification of a thunderstorm and eventual lightning production (Workman and Reynolds 1949; Reynolds et al. 1957; Takahashi 1978; Williams and Lhermitte 1983; Dye et al. 1988; Saunders et al. 1991; Carey and Rutledge 1996; Blyth et al. 2001; Petersen and Rutledge 2001). Recent observational and modeling work has examined the relationship between ice content or flux and lightning flash rates and found a strong correlation between precipitation ice mass or graupel volume/fluxes and CG and total lightning (CG plus intracloud lightning; Nesbitt et al. 2000; Petersen and Rutledge 2001; Blyth et al. 2001; Latham et al. 2004; Deierling et al. 2005;

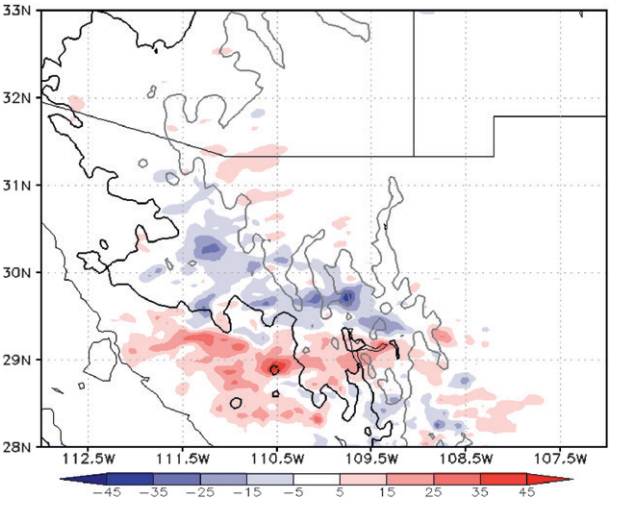

FIG. 12. TUTT − No_TUTT cumulative precipitation differences (mm) between 1800 UTC 12 Jul and 1200 UTC 13 Jul. The narrow black contour denotes the 0-m terrain height along with 500 m (thick black) and 1000 m (gray).

TABLE 1. Mean total precipitation (kg) between 1800 UTC 12 Jul and 1200 UTC 13 Jul for the TUTT and No_TUTT simulations in the region defined by Fig. 12.

	Low	Middle	High	Tot
TUTT	1.40×10^{16}	1.49×10^{16}	2.59×10^{16}	5.48×10^{16}
No_TUTT	5.58×10^{15}	1.95×10^{16}	1.92×10^{16}	4.42×10^{16}

Petersen et al. 2005; Wiens et al. 2005; Latham et al. 2007; Deierling et al. 2008). Specifically of interest to this study, Deierling et al. (2008) show a strong correlation between graupel fluxes and total and CG lightning. Figure 14 displays the mean graupel mixing ratio for grid points having vertical velocities greater than 1 m s^{-1}, over the region in Fig. 12, and only for model levels between 0°C and −20°C, which can be used as an estimate of the ''charging zone'' (Latham et al. 2004; Deierling et al. 2008). The 1 m s^{-1} threshold was used as a simple way to examine only grid points with ''convective'' updrafts. It is evident that the TUTT simulations generate more charging zone graupel between 2100 UTC 12 July and 0000 UTC 13 July than the No_TUTT simulations, which corresponds to the time period of strongest updrafts (Fig. 11).

Because of these simulations being performed at 4-km horizontal resolution, likely producing updrafts that are too broad and weak (Bryan et al. 2003; Bryan and Morrison 2012), no effort is made to produce quantitative graupel or ice mass fluxes and corresponding estimated lightning counts. As a qualitative estimate of graupel flux in the charging zone, Fig. 15 displays the product of the charging zone average graupel mixing ratio and charging zone average vertical velocities. The TUTT simulation mean has more graupel flux over most active period (2100 UTC 12 July–0000 UTC 13 July) and more cumulative graupel flux over the entire period. Increased charging zone graupel (Fig. 14) along with stronger maximum updrafts (Fig. 11) and qualitatively more graupel flux (Fig. 15), suggests more vigorous graupel growth and a noninductive charging mechanism in the TUTT simulations (Latham et al. 2004; Deierling et al. 2008).

Finally there is some observational support for the simulated microphysical differences between the TUTT and No_TUTT simulations. Lang et al. (2010) examine S-band dual-polarization Doppler radar (SPOL) data for the NAME period and produce statistics for precipitation ice and liquid water mass. They segment their data into terrain bands and by regime. Lang et al. (2007) had previously defined a disturbed regime in which convection more readily organizes and propagates off and along the SMO. Most importantly, disturbed days have increased shear at coastal sounding sites, which also happens with TUTT occurrence. For disturbed days, Lang et al. (2010) find that for terrain less than 1500 m,

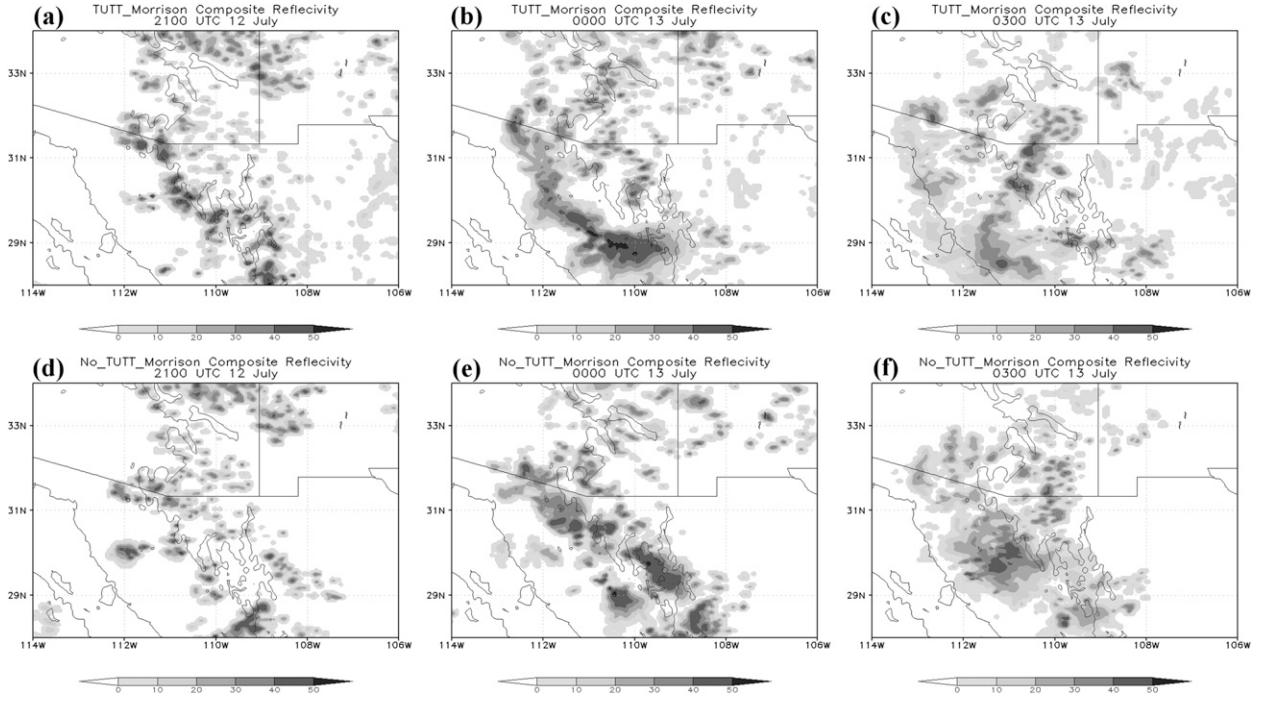

FIG. 13. Simulated composite radar reflectivity (dBZ) from the (a)–(c) TUTT and (d)–(f) No_TUTT simulations using the Morrison microphysics scheme at (a),(d) 2100 UTC 12 Jul; (b),(e) 0000 UTC 13 Jul; and (c),(f) 0300 UTC 13 Jul.

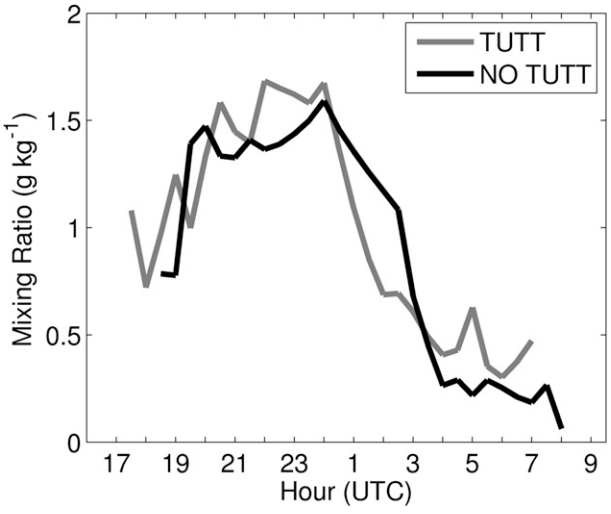

FIG. 14. Average graupel mixing ratio (g kg^{-1}) in the region defined by Fig. 12 for all grid points with $w > 1$ m s^{-1} between the 0° and −20°C isotherms. The time series runs from 1600 UTC 12 Jul to 1000 UTC 13 Jul.

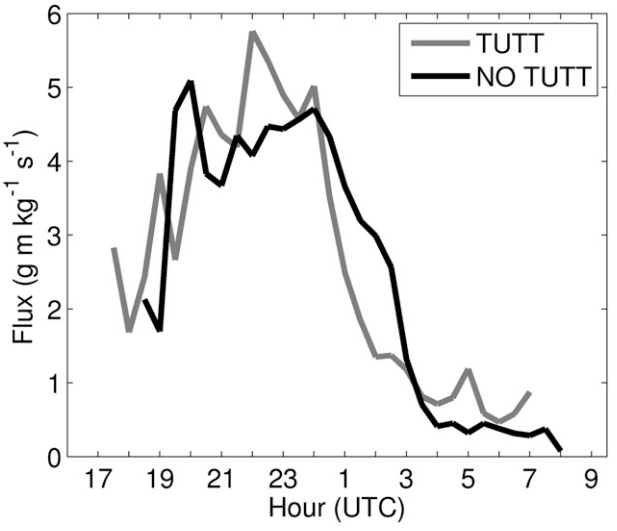

FIG. 15. Qualitative average graupel flux (g m kg^{-1} s^{-1}) for the charging zone for the same grid points in Fig. 14.

extending onto the coastal plain and into the GoC, there is an increase in ice mass with the largest increases in ice mass in the mixed phase layer, where ice mass includes include snow, graupel, and hail. There is also a slight increase in liquid water mass extending above the 0°C isotherm, which will enhance graupel production (Reisner et al. 1998; Thompson et al. 2008). These findings support the simulated differences discussed above. While these results are for the southern SMO, they may be directly applicable to the northern SMO, only about 500 km from the SPOL.

5. Impacts on surge evolution

The gulf surge on 13–14 July was a strong surge event that initiated near the mouth of the GoC and propagated up the GoC channel throughout the day (Rogers and Johnson 2007). With the surge event initiated by large-scale features and being impacted by convection along the SMO (Rogers and Johnson 2007), both simulation sets contain the surge. This study focuses on convective modifications along the northern GoC, so the discussion will be limited to impacts on the environment and surge event in that region.

Comparisons between the TUTT and No_TUTT simulations have shown that there is more organized convection, precipitation, and graupel along the northern SMO in the TUTT simulations. This implies that the TUTT simulations may have more extensive cold pools due to increased evaporation and melting. Figure 16 displays potential temperature differences between the TUTT and No_TUTT simulations. At 2200 UTC (Fig. 16a), the TUTT simulations are beginning to produce more extensive cold pools (blue shading) along the northern SMO. At this point there has been more precipitation (not shown) and graupel production (Fig. 14) in the TUTT simulations over this region. This trend continues through 0200 UTC 13 July (Fig. 16b). The TUTT simulations have had more cumulative precipitation and graupel production up to this point and have established a large consolidated outflow. It is possible that differences in low-level temperature and humidity (Figs. 9a,b) would give rise to differing evaporative cooling environments besides just increased precipitation. From Figs. 9a,b, the TUTT simulations appear to have a low-level environment more conducive to evaporative cooling, which in conjunction with increased precipitation and graupel production would further aid the development of stronger cold pools. At 0600 UTC (Fig. 16c), the TUTT simulations have a generally colder environment along the SMO due to the more extensive cold pool production prior to this time and the expansion of the larger cold pools in the TUTT simulations. By 1000 UTC 13 July (Fig. 16d) it is interesting to note a large area where the No_TUTT simulations are colder. This is actually the surge signal propagating up the GoC in the No_TUTT simulations.

Figure 16 indicates that the TUTT simulations may have a stronger surge event in the northern GoC than the No_TUTT simulations, based on the results of Stensrud et al. (1997), which showed that surge events are weaker without any convection. This behavior is confirmed in Fig. 17, which displays the areal average precipitable water (PW) over the extreme northern GoC over the course of 13 July. Changes in PW correlate well with the

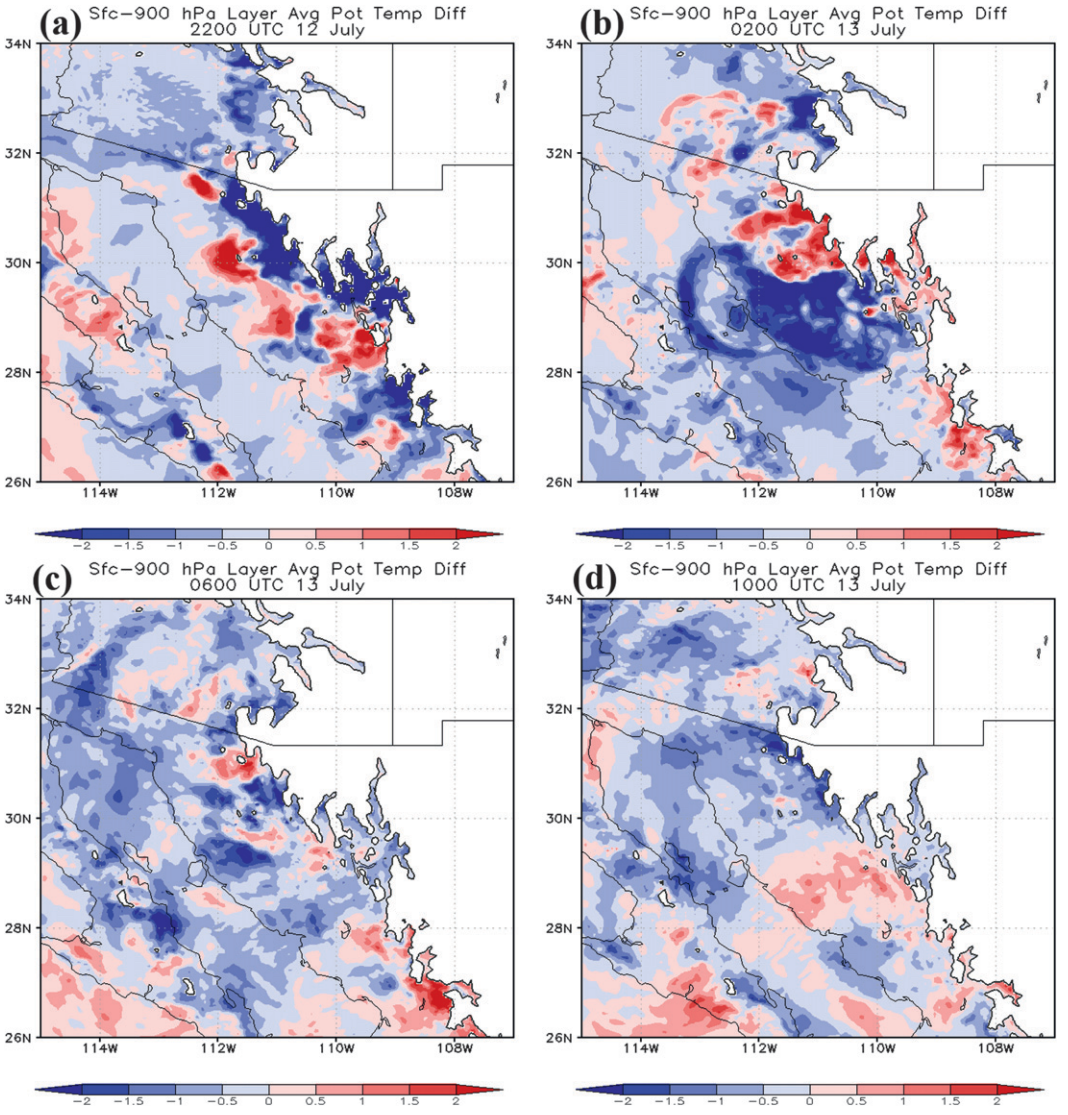

FIG. 16. Surface–900-hPa layer average potential temperature differences (TUTT − No_TUTT) (K) at (a) 2200 UTC 12 Jul, (b) 0200 UTC 13 Jul, (c) 0600 UTC 13 Jul, and (d) 1000 UTC 13 Jul. The white areas are above 900 hPa. The TUTT center is to the left of the displayed area, near 26°–27°N, 105°W.

net moisture flux at a point or over a region, thus it is a good indicator of the moistening ability of a surge event. Since surges are primarily low-level features, the PW from only the lowest 30 hPa is examined in an attempt to focus on surge-related moistening only. Figure 17 shows that the TUTT-mean PW begins to increase earlier and reaches a higher maximum than the No_TUTT simulations. It is interesting to note that by 0000 UTC 14 July, the two simulation sets have nearly identical PW values. This suggests that in this case, changes in convective intensity in the northern GoC modulate the initial surge strength, while the convection in the southern GoC and large-scale forcing features drive the general surge characteristics.

6. Summary

Tropical upper-tropospheric troughs (TUTTs) in the NAM region are unique because they have enhanced precipitation on the western side (Douglas and Englehart 2007; Bieda et al. 2009; Finch and Johnson 2010), while TUTTs throughout the rest of the world typically have enhanced precipitation on the eastern flank (Erickson 1971; Kelly and Mock 1982; Chen and Chou 1994; Whitfield and Lyons 1992). Finch and Johnson (2010) found that enhanced shear in the 700–400-hPa layer had the highest correlation with increased convection for the 12–13 July 2004 TUTT that occurred during the North American Monsoon Experiment (NAME) and

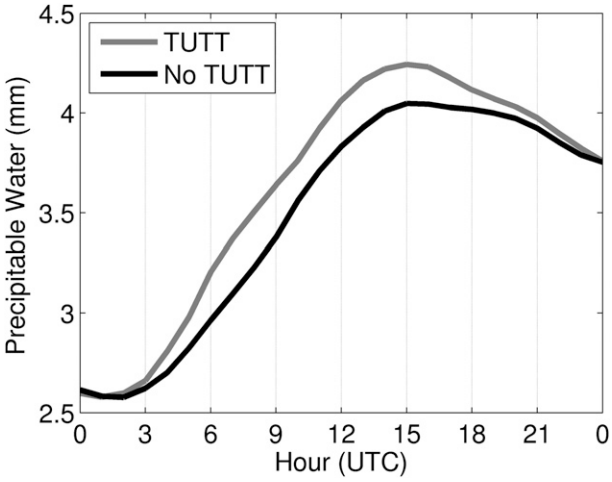

FIG. 17. Areal average of precipitable water (mm) for 0000 UTC 13 Jul–0000 UTC 14 Jul in the lowest 30 hPa above ground over the box bounded by 31°–34°N and 115°–113°W.

found quasigeostrophic diagnosed subsidence in the western side in apparent contradiction to the enhanced convection in that region.

This study examines the 12–13 July case further, focusing specifically on the dynamical and microphysical mechanisms associated with the TUTT and its accompanying convection. The use of a modified vorticity-removal algorithm within the ARW-WRF, usually applied to bogussing tropical cyclone centers, allows for the removal of the vorticity anomaly associated with the TUTT in the initial conditions. Six simulations, three with the TUTT (TUTT) and three without (No_TUTT) using different microphysical parameterizations [i.e., the Thompson hybrid single moment, WRF Single-Moment 6-class (WSM6), and the Morrison double moment] are started from the same initial conditions (except for the TUTT-removal portion), permitting examination of TUTT influences on convection and the gulf surge.

The simulations show that there is no enhancement of upper-level rising motion along the SMO in the TUTT simulations as compared to the No_TUTT simulations. The TUTT simulations do show enhanced 700–400-hPa and surface–500-hPa shear along the central and northern SMO late on 12 July, in agreement with Finch and Johnson (2010). The TUTT simulations also show slight increases (on the order of 100 J kg^{-1}) in CAPE, primarily along the SMO foothills. Some slight midlevel cooling was found in the sounding analysis of Finch and Johnson (2010), but the large CAPE changes due to the surge event on 13 July and lack of sounding sites near the SMO foothills prevented conclusive evidence in their study that the TUTT affected CAPE as well as shear. The TUTT simulations show that a combination of slightly increased shear and CAPE along the northern SMO results in more organized and robust convection. This result clarifies how TUTTs uniquely modify precipitation in the NAM region.

The TUTT simulations produce 16% more precipitation than the No_TUTT simulations along the northern SMO between 1800 UTC 12 July and 1200 UTC 13 July, when the TUTT is influencing the northern SMO. Breaking down precipitation into three terrain categories, low: <500 m, middle: between 500 and 1000 m, and high: >1000 m, the TUTT simulation produces 125% more, 23% less, and 16% more for the categories, respectively. The differences between height bands implies that the TUTT simulations produce slightly more initial convection over the high terrain, that convection propagates more rapidly toward the lower terrain, and hence precipitates less over the slopes of the SMO as it moves quickly toward the lower terrain. Assessment of simulated radar reflectivity loops confirms this finding. The TUTT simulations also produce precipitation over a larger area and have a larger mean accumulation per unit area.

There are also microphysical differences between the two simulation sets. The TUTT simulations produce more graupel, cloud ice, and supercooled liquid water between 1600 UTC 12 July and roughly 0000 UTC 13 July. Prior work has shown a strong correlation between CG and total lightning counts to graupel volume and/or ice mass flux in the charging zone (Nesbitt et al. 2000; Petersen and Rutledge 2001; Deierling et al. 2005; Petersen et al. 2005; Wiens et al. 2005; Latham et al. 2007; Deierling et al. 2008). The increased graupel and qualitative ''graupel flux'' in the TUTT simulations suggest a more active charging zone and stronger noninductive charging process and an increase in CG lightning (Wiens et al. 2005; Latham et al. 2007; Deierling et al. 2008). The simulated microphysical changes have observational support from Lang et al. (2010), who use SPOL polarimetric radar data to derive hydrometeor statistics for the NAME period. They find statistically significant increases in ice mass on days with enhanced shear that are the largest in the mixed phase region, along with slight increases in liquid water above the freezing level.

The aforementioned processes also result in the weaker simulated surge in the No_TUTT simulations on 13 July. Convection is intimately linked to surge initiation and evolution as shown in this study and others (e.g., Stensrud et al. 1997). Since TUTTs modulate convection it is logical that they also modulate surge strength. The TUTT simulations produce more convective outflow through the combination of enhanced precipitation, graupel production, and low-level environmental changes.

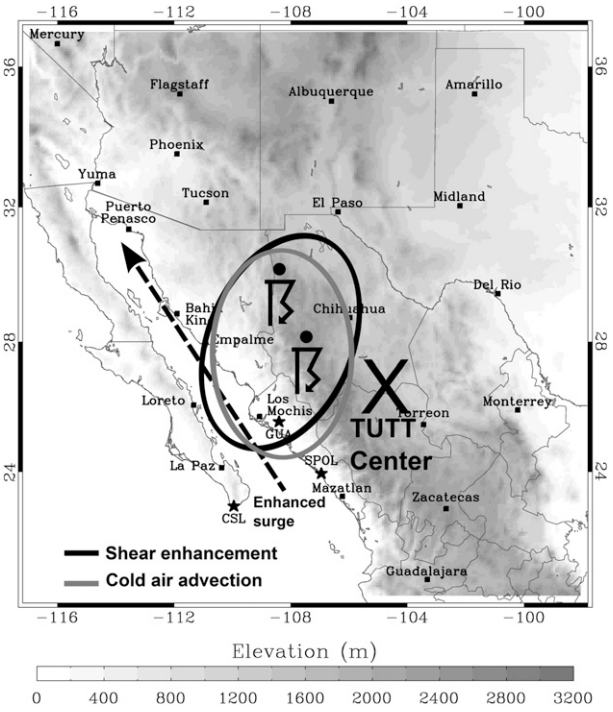

FIG. 18. General schematic diagram of where the TUTT enhances convection and the gulf surge on 12–13 Jul. The large X denotes the TUTT center around 0000 UTC 13 Jul 2004. The black ellipse gives the general area of shear enhancement, while the gray ellipse is the area of midlevel cold air advection from Finch and Johnson (2010). The heavy thunderstorm symbols give the general location of vigorous convective clusters.

This leads to more melting ice mass and evaporation, leading to increased cold air production and larger cold pools. Enhanced midlevel shear supports more organized convection that propagates farther off the SMO and produces more precipitation. It also helps to partially balance the vorticity created by more intense cold pools (Rotunno et al. 1988; Weisman and Rotunno 2004). An analysis similar to that of Bieda et al. (2009) investigating surge duration and/or intensity and TUTTs, in conjunction with these results, could robustly link TUTTs and surge characteristics in the northern GoC and desert Southwest.

Figure 18 presents a general overview, as elucidated from the numerical simulations of the specific TUTT examined herein, which may be applicable to other TUTTs in the NAM region. The TUTT center around 0000 UTC 13 July is just east of the SMO, with the western semicircle impacting mainly the northern SMO. The gray ellipse highlights the general area of midlevel cold air advection and quasigeostrophic diagnosed sinking motion in Finch and Johnson (2010) as well areas of slightly enhanced CAPE and sinking motion from this study. The black ellipse denotes the areas of enhanced surface–500-hPa and 700–400-hPa shear found in this study and Finch and Johnson (2010). The heavy thunderstorm symbols denote the general areas of observed and simulated organized convection around 0300 UTC 13 July. The areas of organized convection coincide with the areas of cold air advection, increased CAPE, and shear along the western semicircle of the TUTT. This combination of features: midlevel sinking motion, cold air advection, enhanced shear, and increased CAPE would not necessarily enhance precipitation, especially in areas without a surface trigger (i.e., oceanic regions), but the SMO provides daily triggering via strong surface heating and solenoidal circulations. Incipient updrafts experience the more favorable convective conditions and evolve to produce more vigorous convection with enhanced precipitation and microphysical differences versus non-TUTT days.

Acknowledgments. The authors thank Paul Ciesielski, Chris Davis, Brian McNoldy, and Rick Taft for all their assistance relating to this research. The comments of three anonymous reviewers are also greatly appreciated. This work was supported by NASA Headquarters under NASA contracts NNX07AD35G and NNX10AG81G and by the National Science Foundation, by both the Mesoscale Dynamic Meteorology Program, under Grant ATM-0639461, and the Physical and Dynamic Meteorology Program, under Grant AGS-0966758. Also, we would like to acknowledge high-performance computing support provided by NCAR's Computational and Information Systems Laboratory, sponsored by the National Science Foundation.

REFERENCES

Bieda, S. W., III, C. L. Castro, S. L. Mullen, A. C. Comrie, and E. Pytlak, 2009: The relationship of transient upper-level troughs to variability of the North American monsoon system. *J. Climate,* **22,** 4213–4227.

Bluestein, H. B., 1992: *Synoptic-Dynamic Meterology in Midlatitudes*. Vol. 1, *Principles of Kinematics and Dynamics,* Oxford University Press, 431 pp.

Blyth, A. M., H. J. Christian, K. Driscoll, A. M. Gadian, and J. Latham, 2001: Determination of ice precipitation rates and thunderstorm anvil ice contents from satellite observations of lightning. *Atmos. Res.,* **59–60,** 217–229.

Brenner, I. S., 1974: A surge of maritime tropical air-Gulf of California to the southwestern United States. *Mon. Wea. Rev.,* **102,** 375–389.

Bruyere, C., and Coauthors, 2010: Weather Research and Forecasting ARW version 3 modeling system user's guide. Mesoscale and Microscale Meteorology Division, National Center for Atmospheric Research, 312 pp.

Bryan, G. H., and H. Morrison, 2012: Sensitivity of a simulated squall line to horizontal resolution and parameterization of microphysics. *Mon. Wea. Rev.,* **140,** 202–225.

——, J. C. Wyngaard, and J. M. Fritsch, 2003: Resolution requirements for the simulation of deep moist convection. *Mon. Wea. Rev.,* **131,** 2394–2416.

——, J. C. Knievel, and M. D. Parker, 2006: A multimodel assessment of RKW theory's relevance to squall-line characteristics. *Mon. Wea. Rev.,* **134,** 2772–2792.

Byers, H. R., and R. R. Braham, 1948: Thunderstorm structure and circulation. *J. Meteor.,* **5,** 71–86.

Carey, L. D., and S. A. Rutledge, 1996: A multiparameter radar case study of the microphysical and kinematic evolution of a lightning producing storm. *J. Meteor. Atmos. Phys.,* **59,** 33–64.

Chappell, C. F., 1986: Quasi-stationary convective events. *Mesoscale Meteorology and Forecasting,* P.S. Ray, Ed., Amer. Meteor. Soc., 289–309.

Chen, G. T. J., and L. F. Chou, 1994: An investigation of cold vortices in the upper troposphere over the western North Pacific during the warm season. *Mon. Wea. Rev.,* **122,** 1436–1448.

Coniglio, M. C., D. J. Stensrud, and L. J. Wicker, 2006: Effects of upper-level shear on the structure and maintenance of strong quasi-linear mesoscale convective systems. *J. Atmos. Sci.,* **63,** 1231–1252.

Corfidi, S. F., 2003: Cold pools and MCS propagation: Forecasting the motion of downwind-developing MCSs. *Wea. Forecasting,* **18,** 997–1017.

Cotton, W. R., G. H. Bryan, and S. C. van den Heever, 2010: *Storm and Cloud Dynamics*. 2nd ed. Academic Press, 820 pp.

Crook, N. A., 1996: Sensitivity of moist convection forced by boundary layer processes to low-level thermodynamic fields. *Mon. Wea. Rev.,* **124,** 1767–1785.

Cummins, K. L., M. J. Murphy, E. A. Bardo, W. L. Hiscox, R. B. Pyle, and A. E. Pifer, 1998: A combined TOA/MDF technology upgrade of the U.S. National Lightning Detection Network. *J. Geophys. Res.,* **103** (D8), 9035–9044.

Deierling, W., W. A. Petersen, J. Latham, S. M. Ellis, and H. J. Christian, 2005: On the relationship of thunderstorm ice hydrometeor characteristics and total lightning measurements. *Atmos. Res.,* **76,** 114–126.

——, ——, ——, ——, and ——, 2008: The relationship between lightning activity and ice fluxes in thunderstorms. *J. Geophys. Res.,* **113,** D15210, doi:10.1029/2007JD009700.

Douglas, A. V., and P. J. Englehart, 2007: A climatological perspective of transient synoptic features during NAME 2004. *J. Climate,* **20,** 1947–1954.

Dye, J. E., J. J. Jones, A. J. Weinheimer, and W. P. Winn, 1988: Observations within two regions of charge during initial thunderstorm electrification. *Quart. J. Roy. Meteor. Soc.,* **114,** 1271–1290.

Erickson, C. O., 1971: Diagnostic study of a tropical disturbance. *Mon. Wea. Rev.,* **99,** 67–78.

Farfán, L. M., and J. A. Zehnder, 1994: Moving and stationary mesoscale convective systems over northwest Mexico during the Southwest Area Monsoon Project. *Wea. Forecasting,* **9,** 630–639.

Finch, Z. O., and R. H. Johnson, 2010: Observational analysis of an upper-level inverted trough during the 2004 North American Monsoon Experiment. *Mon. Wea. Rev.,* **138,** 3540–3555.

Fredrick, S., C. Davis, D. Gill, and S. Low-Nam, 2009: Bogussing of tropical cyclones in WRF version 3.1. Tech. Doc. P1.5, National Center for Atmospheric Research, 6 pp. [Available online at http://www.mmm.ucar.edu/wrf/users/workshops/WS2009/abstracts/P1-05.pdf.]

Hales, J. E., Jr., 1972: Surges of maritime tropical air northward over the Gulf of California. *Mon. Wea. Rev.,* **100,** 298–306.

Hong, S.-Y., and J.-O. J. Lim, 2006: The WRF single-moment 6-class microphysics scheme (WSM6). *J. Korean Meteor. Soc.,* **42,** 129–151.

Kelly, W. E., Jr., and D. R. Mock, 1982: A diagnostic study of upper tropospheric cold lows over the western North Pacific. *Mon. Wea. Rev.,* **110,** 471–480.

Lang, T. J., D. A. Ahijevch, S. W. Nesbitt, R. E. Carbone, S. A. Rutledge, and R. Cifelli, 2007: Radar-observed characteristics of precipitating systems during NAME 2004. *J. Climate,* **20,** 1713–1733.

——, S. A. Rutledge, and R. Cifelli, 2010: Polarimetric radar observations of convection in northwestern Mexico during the North American Monsoon Experiment. *J. Hydrometeor.,* **11,** 1345–1357.

Latham, J., A. M. Blyth, H. J. Christian Jr., W. Deierling, and A. M. Gadian, 2004: Determination of precipitation rates and yields from lightning measurements. *J. Hydrol.,* **288,** 13–19.

——, W. A. Petersen, W. Deierling, and H. J. Christian, 2007: Field identification of a unique globally dominant mechanism of thunderstorm electrification. *Quart. J. Roy. Meteor. Soc.,* **133,** 1453–1457.

Li, J., S. Sorooshian, W. Higgins, X. Gao, B. Imam, and K. Hsu, 2008: Influence of spatial resolution on diurnal variability during the North American monsoon. *J. Climate,* **21,** 3967–3988.

Lin, Y.-L., R. D. Harley, and H. D. Orville, 1983: Bulk parameterization of the snow field in a cloud model. *J. Climate Appl. Meteor.,* **22,** 1065–1092.

Mesinger, F., and Coauthors, 2006: North American Regional Reanalysis. *Bull. Amer. Meteor. Soc.,* **87,** 343–360.

Morrison, H., J. A. Curry, and V. I. Khvorostyanov, 2005: A new double-moment microphysics parameterization for application in cloud and climate models. Part I: Description. *J. Atmos. Sci.,* **62,** 1665–1677.

——, G. Thompson, and V. Tatarskii, 2009: Impact of cloud microphysics on the development of trailing stratiform precipitation in a simulated squall line: Comparison of one- and two-moment schemes. *Mon. Wea. Rev.,* **137,** 991–1007.

Nesbitt, S. W., E. J. Zipser, and D. J. Cecil, 2000: A census of precipitation features in the tropics using TRMM: Radar, ice scattering, and lightning observations. *J. Climate,* **13,** 4087–4106.

Petersen, W. A., and S. A. Rutledge, 2001: Regional variability in tropical convection: Observations from TRMM. *J. Climate,* **14,** 3566–3596.

——, H. J. Christian, and S. A. Rutledge, 2005: TRMM observations of the global relationship between ice water content and lightning. *Geophys. Res. Lett.,* **32,** L14819, doi:10.1029/2005GL023236.

Pytlak, E., M. Goering, and A. Bennett, 2005: Upper tropospheric troughs and their interaction with the North American monsoon. Preprints, *19th Conf. on Hydrology,* San Diego, CA, Amer. Meteor. Soc., JP2.3. [Available online at http://ams.confex.com/ams/Annual2005/techprogram/paper_85393.htm.]

Reisner, J., R. M. Rasmussen, and R. T. Bruintjes, 1998: Explicit forecasting of supercooled liquid water in winter storms using the MM5 forecast model. *Quart. J. Roy. Meteor. Soc.,* **124,** 1071–1107.

Reynolds, S. E., M. Brook, and M. F. Gourley, 1957: Thunderstorm charge separation. *J. Meteor.,* **14,** 163–178.

Rogers, P. J., and R. H. Johnson, 2007: Analysis of the 13–14 July gulf surge event during the 2004 North American Monsoon Experiment. *Mon. Wea. Rev.,* **135,** 3098–3117.

Rotunno, R., J. B. Klemp, and M. L. Weisman, 1988: A theory for strong, long-lived squall lines. *J. Atmos. Sci.,* **45,** 463–485.

Sadler, J. C., 1967: The tropical upper tropospheric trough as a secondary source of typhoons and a primary source of trade-wind disturbances. Hawaii Institute of Geophysics Rep. 67-12, 103 pp. [Available from Hawaii Institute of Geophysics, 2525 Correa Rd., Honolulu, HI 96822.]

Saunders, C. P. R., W. D. Keith, and R. P. Mitzeva, 1991: The effect of liquid water on thunderstorm charging. *J. Geophys. Res.,* **96,** 11 007–11 017.

Smith, W. P., and R. L. Gall, 1989: Tropical squall lines of the Arizona monsoon. *Mon. Wea. Rev.,* **117,** 1553–1569.

Stensrud, D. J., R. L. Gall, and M. K. Nordquist, 1997: Surges over the Gulf of California during the Mexican monsoon. *Mon. Wea. Rev.,* **125,** 417–437.

Takahashi, T., 1978: Riming electrification as a charge generation mechanism in thunderstorms. *J. Atmos. Sci.,* **35,** 1536–1548.

Thompson, G., P. R. Field, R. M. Rasmussen, and W. D. Hall, 2008: Explicit forecasts of winter precipitation using an improved bulk microphysics scheme. Part II: Implementation of a new snow parameterization. *Mon. Wea. Rev.,* **136,** 5095–5115.

Thorncroft, C. D., B. J. Hoskins, and M. E. McIntyre, 1993: Two paradigms of baroclinic-wave life-cycle behavior. *Quart. J. Roy. Meteor. Soc.,* **119,** 17–55.

Weisman, M. L., and R. Rotunno, 2004: ''A theory for strong long-lived squall lines'' revisited. *J. Atmos. Sci.,* **61,** 361–382.

Whitfield, M. B., and S. W. Lyons, 1992: An upper-level low over Texas during summer. *Wea. Forecasting,* **7,** 89–106.

Wiens, K. C., S. A. Rutledge, and S. A. Tessendorf, 2005: The 29 June 2000 supercell observed during STEPS. Part II: Lightning and charge structure. *J. Atmos. Sci.,* **62,** 4151–4177.

Williams, E. R., and R. M. Lhermitte, 1983: Radar tests of the precipitation hypothesis for thunderstorm electrification. *J. Geophys. Res.,* **88** (C15), 10 984–10 992.

Workman, E. J., and S. E. Reynolds, 1949: Electrical activity as related to thunderstorm cell growth. *Bull. Amer. Meteor. Soc.,* **30,** 142–149.